Impact of Overhead Excavation on an Existing Shield Tunnel: Field Monitoring and a Full 3D Finite Element Analysis

F. Wang[1,2], D.M. Zhang[1,2,3], H.H. Zhu[4], H.W. Huang[1,2], J.H. Yin[5]

Abstract: This paper studies the impact of overhead excavation on an existing tunnel through both field monitoring and a full 3D numerical model. It is found that the excavation induced longitudinal heave of the tunnel is uneven with maximum heave occurring below the excavation center. Even at the same cross section, the excavation induced heave is not uniform with the most significant heave occurring at the tunnel crown. The bending moments of the tunnel lining is decreased due to the overhead excavation. The axial forces of the tunnel lining generally decrease except at the tunnel invert. The shear forces of the tunnel increase substantially. The excavation induced tunnel deformation and internal forces may reduce the effectiveness of the waterproof system.

Keywords: Excavation, shield tunnel, monitoring, deformation, internal forces.

1   Introduction

As the underground transportation systems become increasingly large in many cities, it is not uncommon to encounter deep excavations in a close-proximity of existing tunnels, which may cause additional forces and displacements to damage the existing tunnels. For example, the Taipei Rapid Transit System was once damaged by adjacent excavation [Chang, Sun, Duann and Hwang (2001)]. To protect the existing tunnel, the displacement of the existing tunnel caused by the adjacent construction must be strictly controlled. In Singapore, the maximum allowable displacement caused by construction on an existing tunnel is 15 mm [Sharma, Hefny,

[1] Key Laboratory of Geotechnical and Underground Engineering of Minister of Education, Tongji University, Shanghai 200092, China.

[2] Department of Geotechnical Engineering, Tongji University, Shanghai 200092, China.

[3] Corresponding author

[4] School of Earth Sciences and Engineering, Nanjing University, Nanjing 210093, China.

[5] Department of Civil and Structural Engineering, The Hong Kong Polytechnic University, Hong Kong, China.

Zhao and Chan (2001)]. In Shanghai, the maximum displacements of the tunnels caused by any adjacent construction activities are not allowed to be more than 20 mm and the early warning must be issued when the displacement caused by excavation is larger than 10mm.

Many researchers have studied the tunnel displacements induced by adjacent excavations. For instance, through numerical simulation and field monitoring, Liu, Li and Liu (2011) found that soil improvement and the excavation sequence had significant effect on the tunnel displacement during the excavation. Sharma, Hefny, Zhao and Chan (2001) studied the tunnel displacement and distortion caused by adjacent excavations. Doležalová (2001) found that the adjacent excavation could induced very significant tunnel displacement. For a jointed segmental shield tunnel, the joint stiffness is smaller than the segment and hence will experience more displacement than the segment. The excessive displacement of tunnel joint will result in tunnel leakage for tunnel embedded in saturated clay. Zhang, Ma, Huang and Zhang (2012) reported that the tunnel leakage could cause non-negligible long-term tunnel settlement and tunnel squat, which will damage the tunnel performance. Thus, more attention should be paid to the movement of the joints for shield tunnel. However, so far, the researches were more focused on the tunnel displacement, hence few information was available for excavation – induced joint movement and additional force of existing tunnel.

This paper aims to evaluate the impact of excavation above an existing tunnel in terms of the displacements, additional forces and joints movements through a case study in Shanghai. The structure of this paper is as follows. First, the construction site was briefly introduced. Then, the field monitoring program and observed displacements were described, followed by a full 3D FEM simulation. Finally, the impact of excavation on the existing tunnel was assessed based on the field monitored data and 3D FEM results.

2   The site

The case study is about an excavation for the construction of an underpass above an existing shield tunnel. Fig. 1 and Fig. 2 show the profile view and plane view of the construction site, respectively. The excavation was 80 m long, 10 m wide and 8 m deep. The existing shield tunnel is part of the Shanghai metro line 2. The external and internal diameters of the shield tunnel are 6.2 m and 5.5 m, respectively, i.e., the thickness of the concrete segment is 0.35 m. The underpass crossed the existing tunnel with an angle of 55° and an overlapping distance of 12 m. The distance from the excavation bottom to the tunnel crown is 7 m. The stress relief on the existing tunnel due to the above excavation is about 150 kPa, which is almost the half of the overburden pressure on the tunnel. Such a large unloading pressure

may make the tunnel move upwards, resulting in additional forces, cross section deformations, and joints movements of the tunnel, which is of great concern of the tunnel owner. As the excavation is directly above the existing tunnel, which is very rare in practice, little is available in the literature about how the excavation will affect the tunnel.
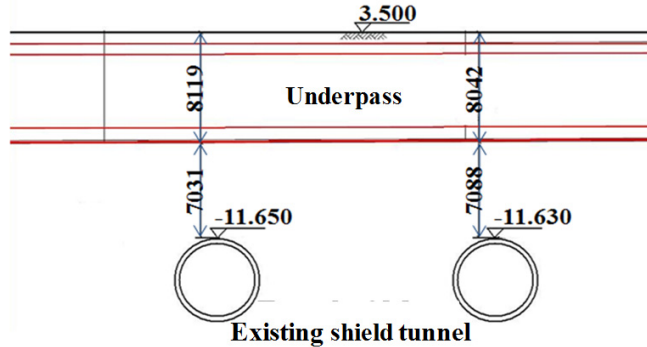
Figure 1: Underpass and the existing shield tunnel (Unit: mm for distance, m for elevation)
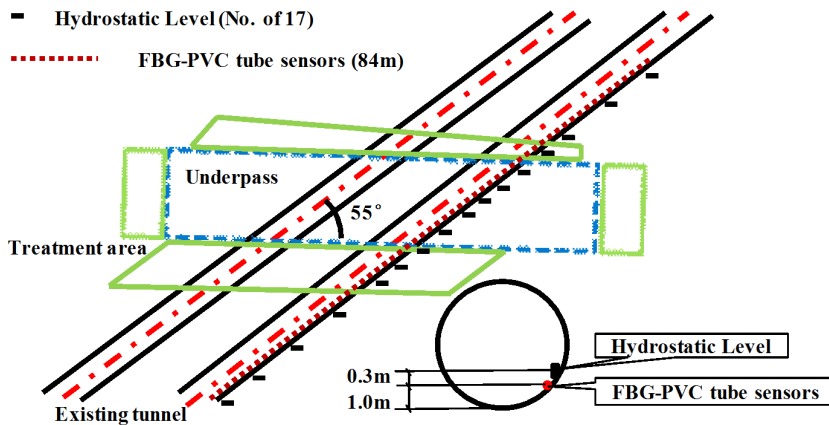
Figure 2: Site plane and layout of the instrumentation

Fig. 3 shows the soil profile at the site and the soil properties are summarized in Tab.1. The soil layer numbers in Fig. 3 and Tab. 1 are named based on local design code. The underground water table is at the ground surface. Hence, the soft clay

is fully saturated. From the ground surface to the bottom of the tunnel are silty clay, clayed silt with sandy silt, mucky clay. The mucky clay is very soft with a compressibility modulus of only 2.3 MPa. As can be seen in Fig. 2, the bottom of the excavation is immediately above the mucky clay, and the upper half part of the tunnel is embedded in the mucky clay. The unloading on this layer due to excavation could result in unexpected heave, cross section deformation and joint movement of the tunnel.

Layer	Soil Type	γ (kN/m^3)	e_0
②	Silty clay	18.5	0.935
③-t	Clayey silt with sandy silt	18.5	0.903
④	Mucky clay	17	1.351
⑤	Silty clay	18.2	0.973
⑥	Silty clay	19.7	0.667
⑦-1	Sandy silt	18.6	0.85
⑦-2	Silty sand	19	0.748
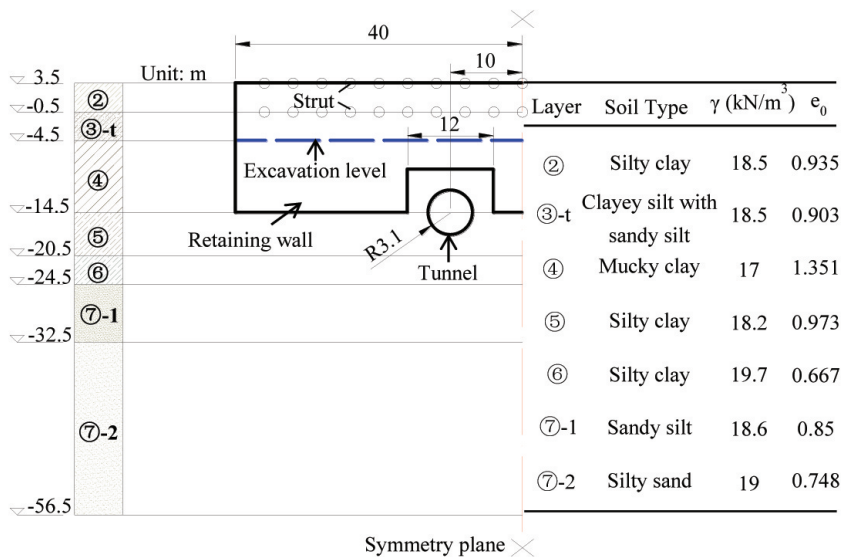
Figure 3: Soil profile (Unit: m)

To reduce the impact of excavation on the underlying existing tunnel, the ground was treated by high pressure jet grouting before excavation. The treated ground ranged from outside the retaining wall to the center of the excavation zone in the plane view and from the ground surface to below the excavation bottom in depth. The construction sequence was as follows:

(1) Construct the 0.68 m thick retaining wall with cast in-place piles up to depth of 18 m. The retaining wall is 12 m deep above the existing tunnel covering a length of 12 m to avoid the tunnel as shown in Fig. 3,

(2) Install the first level strut of steel pipe. The first strut was set at the elevation of ground surface.

(3) Excavate to the depth of 4 m followed by the installation of the second level strut of steel pipe at the same depth.

(4) Excavate to the target depth of 8 m.

During the excavation, The soil was divided by several strips and excavated from the center to the two sides to further reduce its effect on the underlying existing shield tunnel.

Table 1: Properties of soils

Layer No.	Compressibility modulus E_s (MPa)	Coefficient of earth pressure at rest K_0	Poisson's ratio ν	Cohesion c (kPa)	Friction angle ϕ (°)	Coefficient of perme-ability k_s(m/s)
②	4.38	0.5	0.32	17	18.5	1.42E-8
③-t	7.45	0.43	0.3	7	26	5.15E-8
④	2.3	0.65	0.36	13	12.5	3.18E-9
⑤	4.61	0.58	0.33	17	18.5	7.25E-9
⑥	7.81	0.42	0.3	46	18	7.68E-9
⑦-1	11.06	0.36	0.3	4	32	3.24E-6
⑦-2	14.61	0.35	0.3	0	36	1.61E-5

3   Field monitoring of tunnel displacement

The on-site monitoring has been one of the key approaches used to reveal the tunnel behavior due to the adjacent engineering activities. Zhou, Xie, Yang and Jiang (2012) proposed a vibration-based structure health monitoring system (SHMS) for Shanghai shield tunnel to survey the lining safety. However, the application of vibration-based SHMS still remains a big challenge for shield tunnel because the vibration characteristics of shield tunnel is significantly impacted by the soil properties. Ullah, Pichler, Scheiner, and Hellmich (2010) reported that the 3D displacement vectors of tunnel lining could be obtained by laser optical systems. But the huge amount of data gained from laser optical system makes the post-processing very time-consuming. Considering the feasibility of on-site monitoring system, the complex construction sequences and the significant unloading caused by the excavation, the field monitoring of tunnel displacement was carried out with two independent methods, i.e., a newly developed FBG-PVC tube sensor method and the traditional Hydrostatic Level method. The fiber optic sensor method including FBG (Fiber Bragg Grating) method is now widely applied in structure health monitoring for its reliability, high resolution, robustness, and non-electromagnetic influence. [Dunnicliff (1993); Othonos and Kalli (1999); Casas and Cruz (2003); Li, Li and Song (2004); Shivakumar and Bhargava (2004); Chan, Yu, Tam, Ni, Liu,

Chung and Cheng (2006); Glisic and Inaudi (2007)]. Considering the discontinuity of tunnel segmental lining, the FBG-PVC tube sensor method was used to monitor the shield tunnel where the PVC tube was used as the transmitter of the displacement from the measured tunnel to FBGs and the FBGs were adhered to the PVC tube by epoxy resin. [Metje, Chapman, Rogers, Henderson and Beth (2008); Yin, Zhu and Fung (2008); Yin, Zhu, Pei and Hong (2010); Zhu, Ho, Yin, Sun, Pei and Hong (2012)].

3.1 *Instrumentation*

Considering the possible affected zone of the excavation, the FBG – PVC tube sensors were installed symmetrically at every 2m from the excavation center to outside along the tunnel covering a length of 84 m. The Hydrostatic Levels were installed with an interval of 3 m below the excavation bottom and an interval of 5 m outside this range. The total monitored length of the Hydrostatic Level method is also 84 m. In total, 42 FBG – PVC tube sensors and 17 Hydrostatic Levels were installed on the existing tunnel. The FBG-PVC tube sensors and the Hydrostatic Levels were installed at 1 m and 1.3 m above the tunnel invert, respectively. The layout of the instrumentation is shown in Fig. 2. Fig. 4 shows the typical completed monitoring instruments.
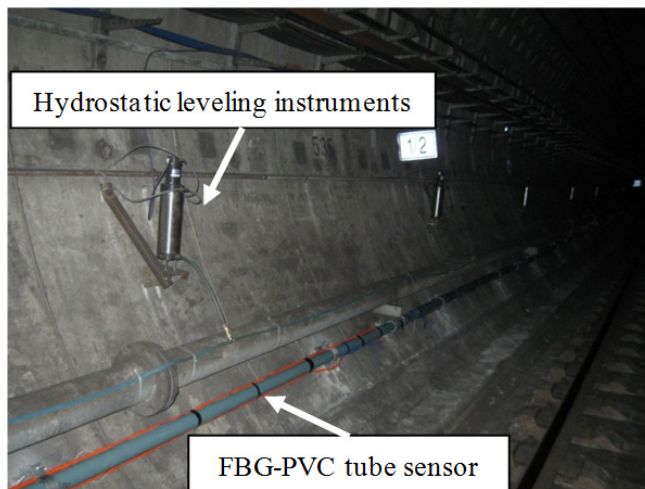
Figure 4: Typical Hydrostatic Level and FBG-PVC tube sensor installed in the tunnel

3.2 Field data

To find out the effect of the excavation on the existing tunnel, the displacements of existing tunnel were measured before the excavation, during the excavation and after the excavation, respectively. The reference monitoring was carried out on 20 Jan. 2009. The excavation was started on 10 Feb. 2009 and completed on 18 Aug. 2009. The post-construction displacements were monitored 9 months after the completion of the excavation on 13 May 2010. Fig. 5 presents the displacements of the underlying existing tunnel due to above excavation measured using the FBG – PVC tube sensor method. It is interesting to observe that the largest heave of the tunnel is 10.36 mm, which occurred when the excavation was completed, and was below the center of the excavation. The tunnel moved back about 1.6 mm in 9 months after the excavation was completed due to the reloading imposed by the underpass structure constructed above the tunnel.

The heaves measured by Hydrostatic Levels are shown in Fig. 6. Comparing Fig. 5 and Fig. 6, the developments of displacement with excavation obtained by the two monitoring systems are similar. The measured maximum heave by the Hydrostatic Levels was 8.95mm, which is slightly smaller than that obtained by FBG – PVC tube sensor method, probably because the installation positions of the two instruments are not exactly the same. Overall, the monitoring results of the two independent monitoring systems are largely consistent, thus verifying the applicability of the FBG-PVC tube sensor method for tunnel deformation. Unlike the Hydrostatic Level method, the cost of the FBG-PVC tube sensor method does not increase with the number of monitoring points.

The observed tunnel displacements from both FBG-PVC tube sensor and the Hydrostatic Level imply that the excavation induced displacement of the tunnel might have exceeded the early warning threshold but is smaller than the allowable maximum displacement set in Shanghai. The recovery of the displacement is about 10% of the resulted displacement after the excavation was completed for nine months. Thus, the impact of the excavation on the underlying tunnel can not be neglected.
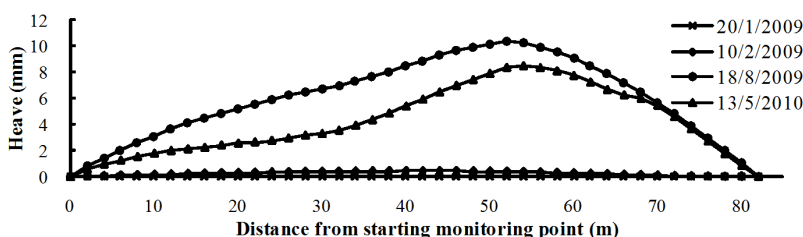
Figure 5: Tunnel heave measured by FBG-PVC tube sensor
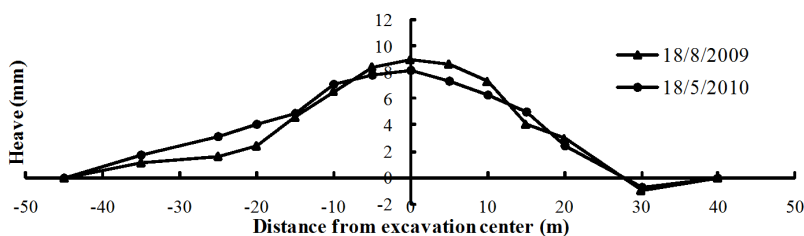
Figure 6: Tunnel heave measured by Hydrostatic Level

4   3D finite element analysis

4.1   3D finite element model

While the field monitored data provide valuable information about the response of the tunnel caused by overhead excavation, it only provides partial knowledge about the tunnel at the selected monitored points. To further study the deformation and internal forces of the tunnel, the excavation process is simulated using a full 3D finite element model with ABAQUS^{TM} [Dassault Systèmes Simulia Corp. (2010)]. Fig. 7 shows the mesh of the model employed in this study. The lateral boundaries were fixed in the horizontal direction but allowed to move vertically. The boundary at the bottom were fixed in both horizontal and vertical directions. To minimize the effect of idealized boundaries, the model was 250 m in length,100 m in width, and 60 m in height. The Mohr-Coulomb constitutive model was used for soils. The Young's modulus of soil was obtained from compressibility modulus based on the experimental data judged with engineering experience. In Shanghai, the ratio of Young's modulus to the compressibility modulus for clay is usually about four to five, and could be even higher for very soft clay [Zhang and Huang (2009)]. For sand, Young's modulus is approximately three times of modulus of compressibility [Brinkgreve, Broere and Waterman (2006)]. The interface between tunnel lining and soil is also taken into account to optimize the numerical modeling. Pellet (2009) presented that the consideration of the contact between tunnel lining support and the surrounding rock medium in numerical simulation can make the calculated stress acting in the lining very close to the measured one. Therefore, the interaction between tunnel lining and soil mass around tunnel is considered through the friction coefficient of 0.4 in the model presented in this paper.

The tunnel lining was made up of pre-cast reinforced concrete. The parameters of tunnel lining are listed in Tab. 2. Each lining consists of 6 jointed segments. As the joints between the segments make a significant reduction of tunnel stiffness, a continuous tunnel model with reduced stiffness was used to simulate the jointed
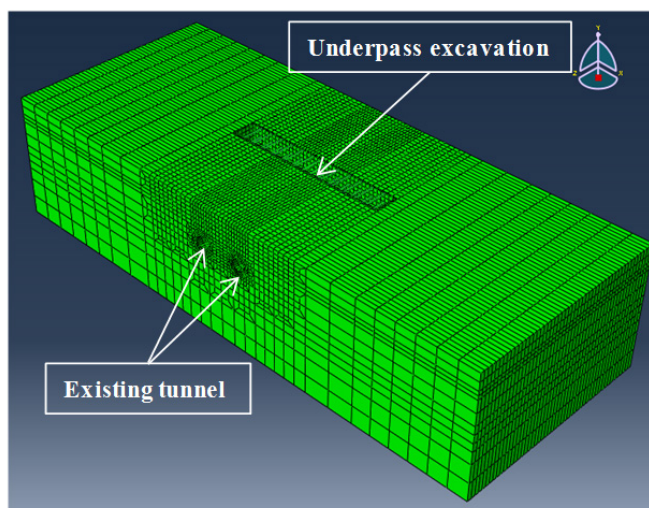
Figure 7: Mesh of the 3D FE model

segmental tunnel . The stiffness reduction method has been widely used in tunnel engineering for simulation of shield tunnels [Shiba, Kawashima, Obinata and Kano (1988); Lee and Ge (2001); Hefny and Chua (2006); Teachavorasinskun and Chub-Uppakarn (2009)]. Based on previous studies for Shanghai shield tunnels [Huang, Xu, Yan and Yu (2006); Cao, Chen and Yang (2008); Liao, Peng and Shen (2008)], the stiffness reduction coefficients for tunnel lining along the circumferential and longitudinal directions are 0.7 and 1/6, respectively. Thus, an orthogonal anisotropy elastic model was adopted to simulate the tunnel lining. Let E_1, E_2, and E_3 denote the Young's modulus in the radial, circumferential and longitudinal directions, respectively. Let E_c denote the Young' modulus of the concrete. The reduced stiffness of the tunnel lining can be obtained by reducing the Young's modulus of the concrete as follows: $E_1 = E_2 = 0.7E_c$, and $E_3 = 1/6E_c$. The shear modulus can be obtained in the same way as Young's modulus [Lekhnitskii (1981); Samanta and Ghosh (2009)]. The properties of the concrete retaining wall was presented in Tab.3. The thickness of retaining wall was 0.68 m. Steel pipes with the outer diameter of 609 mm and inner diameter of 518 mm were used for struts with a horizontal spacing of 5 m. The properties of the struts are presented in Tab.4. The retaining wall and the struts were assumed to be linear elastic.

Here 1, 2 and 3 represents radial, circumferential and longitudinal direction.

The excavation sequence of the excavation was simulated as follows: (1) The first level steel pipe struts were installed at the ground surface elevation before the ex-

Table 2: Parameters for tunnel lining

Unit weight γ (kN/m^3)	Young's modulus			Shear modulus			Poisson's ratio v
	E_1(MPa)	E_2(MPa)	E_3(MPa)	G_1(MPa)	G_2(MPa)	G_3(MPa)	
25	2.5E+4	2.5E+4	5.9E+3	1.1 E+4	3.8 E+3	3.8 E+3	0.167

Table 3: Parameters for retaining wall

Thickness t (m)	Depth H (m)	Unit weight γ (kN/m^3)	Young's modulus E (MPa)	Poisson's ratio v
0.68	12-18	22	3.0E+4	0.167

Table 4: Parameters for steel pipe props

Diameter D (mm)	Thickness t (mm)	Young's modulus E (GPa)	Poisson's ratio v
609	14	200	0.2

cavation; (2) the first 4 m deep soils were excavated followed by the installation of the second struts, and (3) the soils were finally excavated to the depth of 8 m. For simplicity, the tunnel was set to be perpendicular to the excavation in the numerical model.

4.2 *Excavation induced displacements*

The displacement contours of the shield tunnel when the excavation was completed are shown in Fig. 8. The tunnel heaves obtained by Hydrostatic Level, FBG-PVC tube sensor and 3D finite element method (FEM) are compared in Fig. 9 at the time when the excavation was completed. The largest heave obtained from FBG-PVC tube sensor, Hydrostatic Level, and 3D FEM are 10.36 mm, 8.95 mm, and 10.47 mm, respectively. Overall, the predicted heave from 3D FEM is in between the measured heaves using FBG-PVC tube sensor and Hydrostatic Level. The excavation resulted in significant differential heave of the underlying existing tunnel in the longitudinal direction with the maximum tunnel heave observed right below the excavation center. The differential heave along the tunnel may result in the cir-

cumferential joint movement. It seems that the tunnel heave along the longitudinal direction can be described by a Gaussian curve as follows.

$$(x) = S_{max} exp(-x^2/2i^2) \tag{1}$$

in which, x is the distance from the heave center, $S(x)$ is the tunnel heave along the longitudinal direction, S_{max} is the maximum tunnel heave, i is the distance from the center to the inflection point of heave curve. According to Peck (1969), the inflection point at which the curvature changes from positive to negative can be determined by Equation (2):

$$S_{inf} = 0.61 S_{max} \tag{2}$$

in which, S_{inf} is the tunnel heave at the inflection point, S_{max} is the maximum tunnel heave. The calculated inflection point is 20.38 m from the center of heave curve.
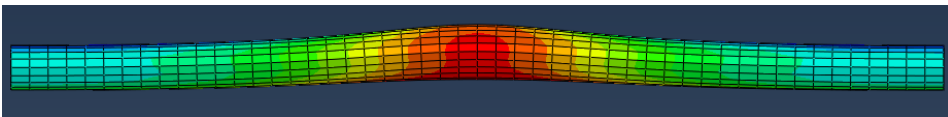
Figure 8: Displacement contour of the tunnel due to overhead excavation
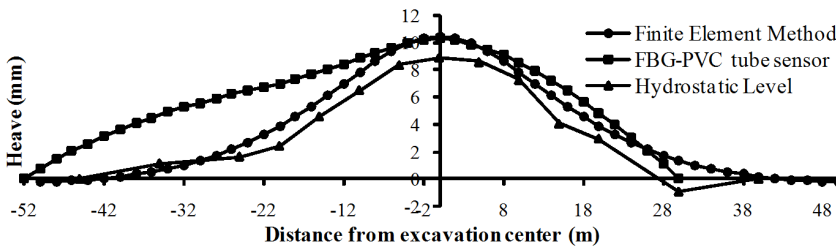
Figure 9: Comparison of tunnel heaves by FEM, FBG-PVC tube sensor and Hydrostatic Level when the excavation was completed

Fig. 10 shows the tunnel heave along the tunnel circumference at different locations. It shows that even at the same cross section the tunnel heave is not uniform with heave increasing from the invert to the crown. For instance, at the cross section of the tunnel below the excavation center, the calculated heaves at the crown and invert are 15.55 mm and 8.14 mm, respectively. In practice, the monitoring instruments are usually installed near the tunnel invert for convenience. As the heave
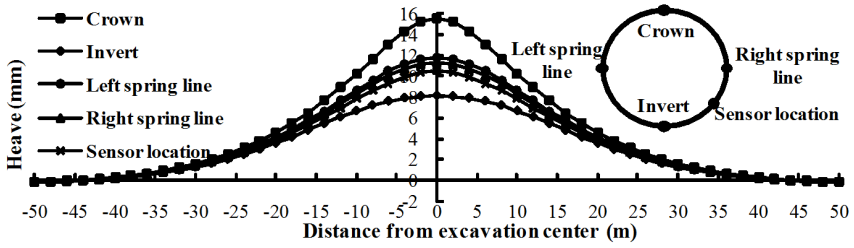
Figure 10: Tunnel heave along longitudinal direction of tunnel at different circumferential locations
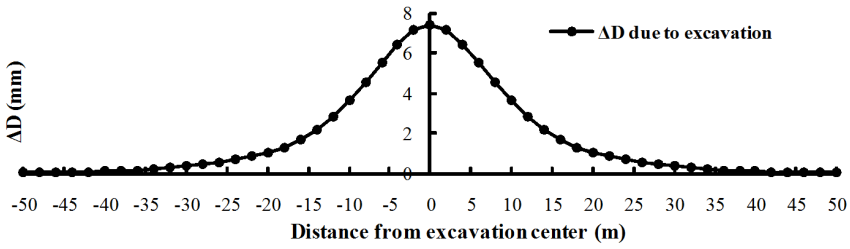
Figure 11: Cross section deformation of tunnel lining
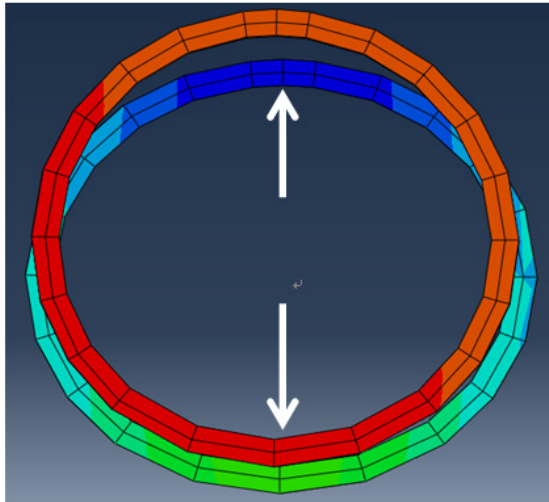
Figure 12: Joint movement due to the nonuniform cross section deformation of tunnel rings

at the tunnel invert is the smallest along the cross section, measuring heave at this point could underestimate the actual maximum heave of the tunnel.

The nonuniform heaves along tunnel circumference will result in the cross section deformation of the tunnel and hence additional internal forces. Fig. 11 shows the diameter change which is an index used to describe the magnitude of cross section deformation in vertical direction when the above excavation was completed. The most significant cross section deformation is 7.4 mm measured under the excavation center. Fig. 11 also shows that the cross section deformation was not uniform along the tunnel, which may result in circumferential joint movement between two segmental rings (as shown in Fig. 12) and thus may potentially damage the tunnel watertightness.

4.3   Excavation induced internal forces

Fig. 13 shows the horizontal and vertical shearing forces along the tunnel caused by circumferential joints movement. The maximum vertical shearing force was about 2000kN and occurred at the inflection point of tunnel heave curve, i.e., the most significant joint movement happened at the inflection point. Consequently, the inflection point was the most possible point to be damaged, and should be monitored with great care during the excavation process .
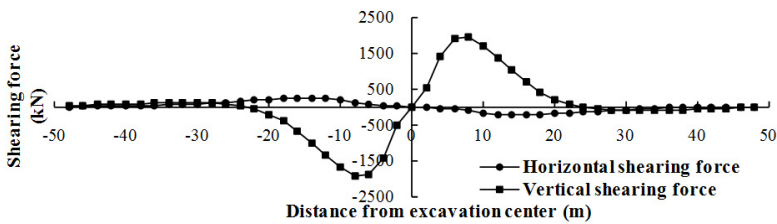
Figure 13: Shearing forces between tunnel rings
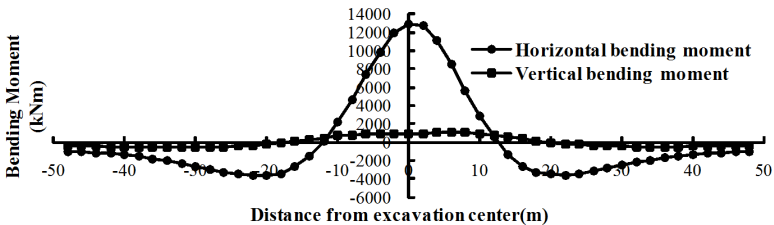
Figure 14: Bending moment along the tunnel

Fig. 14 shows the imposed bending moment along the tunnel caused by the overhead excavation. The longitudinal bending moment could lead to the opening of circumferential joints and thus the increase of the chance of the tunnel leakage.

Fig. 15 presents the initial bending moment before the excavation, after the excavation and the increment in bending moment caused by excavation at crown, invert, left spring line and right spring line of the tunnel ring under the excavation center. Fig. 15 shows that the bending moments decrease significantly due to the unloading caused by overhead excavation. The most significant decrease of bending moment occurred at the tunnel crown with about 91% of the bending moment being decreased. It implies that there is no reduction of the bearing capacity, but movement of joints and water inflow can be predicted due to the excavation.

Fig. 16 shows the initial axial force before the excavation, after the excavation and the increments of axial force by excavation at the crown, invert, left spring line and right spring line of the tunnel below the excavation center. The axial force increased at tunnel invert and decreased at the other three locations. The decrease of axial force is dangerous for the waterproof system as it tends to reduce the compression of rubber gasket placed at the tunnel joints for watertightness. Enough compression of rubber gasket is absolutely essential to keep the tunnel from water inflowing.

The eccentricities of tunnel lining, which is defined as the ratio of bending moment to axial force, at the abovementioned four locations are presented in Fig. 17. Large eccentricities for concrete may cause the lining to crack or may crush the concrete. Fig. 17 shows that the eccentricities increased due to the overhead excavation, particularly at the tunnel crown. Fortunately, the magnitudes of the change in eccentricities are generally small and are unlikely to induce lining crack or crushing of the lining.
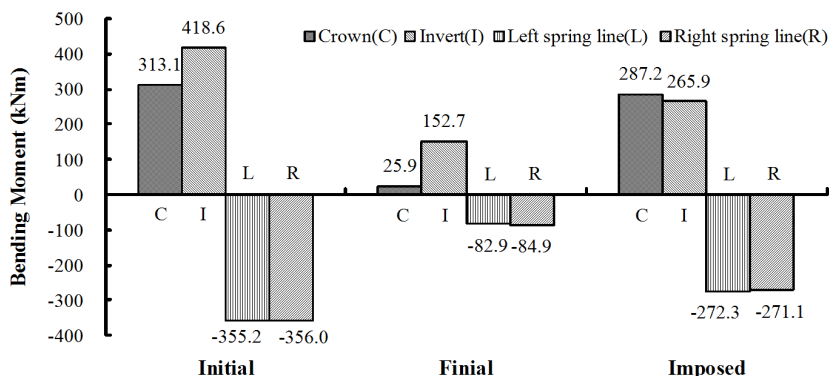
Figure 15: Bending moment of tunnel lining below the excavation center
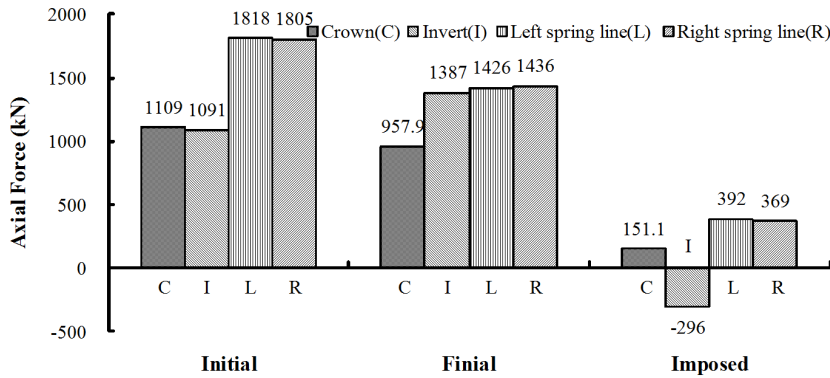
Figure 16: Axial force of tunnel lining under the excavation center
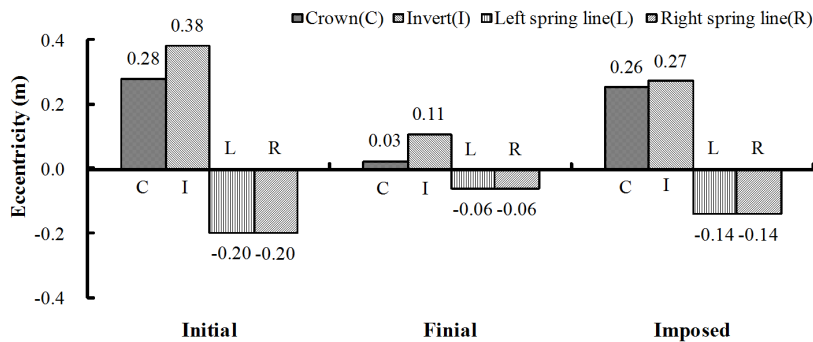
Figure 17: Eccentricity of tunnel lining below the excavation center

5 Summary and Conclusions

This paper studies the impact of overhead excavation on an existing tunnel through both field monitoring and a full 3D finite element analysis. The research reported in this paper and findings from the paper are summarized as follows.

(1) The overhead excavation can induce appreciable impact on the underlying tunnel. The early warning threshold in terms of displacement for protection of the tunnel was violated in the case reported in this paper.

(2) The longitudinal heave of the tunnel caused by the overhead excavation is uneven with maximum heave occurring below the excavation center. The differential longitudinal heave of the tunnel results in the circumferential joint movement. The

most significant joint movement occurred at the inflection point of the heave curve along the tunnel.

(3) Even at the same cross section, the heaves of the tunnel caused by overhead excavation is also uneven, with the most significant heave occurring at the tunnel crown. Within the same cross section, the tunnel heave gradually decreases from the tunnel crown to the invert, leading to cross section deformation of the tunnel. Thus, monitoring the tunnel heave at points other than the tunnel crown may be not conservative.

(4) The bending moments of the tunnel lining is significantly decreased due to the overhead excavation. The axial forces of the tunnel lining generally decrease except at the tunnel invert. The shear forces of the tunnel, however, increases appreciably.

(5) Both the longitudinal uneven heave and the uneven cross section deformation between adjacent tunnel rings can produce the circumferential joint movement, which may potentially reduce the effectiveness of the waterproof system. The decrease of tunnel axial forces may reduce the watertight ability of rubber gasket placed at the circumferential joints for preventing water leakage into the tunnel.

Acknowledgement

References

Brinkgreve, R. B. J.; Broere, W.; Waterman, D. (2006): Plaxis, Finite element code for soil and rock analyses, user's manual. The Netherlands.

Cao, W.H.; Chen, Z.J.; Yang, Z.H. (2008): Study of full-scale horizontal integral ring test for super-large-diameter tunnel lining structure. *The Shanghai Yangtze River Tunnel – Theory, Design and Construction,* Huang R., eds., Taylor and Francis Group, London, pp. 111-123.

Casas, J.R.; Cruz, P.J.S. (2003): Fiber Optic Sensors for Bridge Monitoring. *Journal of Bridge Engineering*, vol. 8, no. 6, pp. 362-373.

Chan, T.H.T.; Yu, L.; Tam, H.Y.; Ni, Y.Q.; Liu, S.Y.; Chung, W.H.; Cheng, L.K. (2006): Fiber Bragg Grating Sensors for Structural Health Monitoring of Tsing Ma Bridge: Background and Experimental Observation. *Engineering Structures*, vol. 28, no. 5, pp. 648-659.

Chang, C.T.; Sun, C.W.; Duann, S.W.; Hwang, R.N. (2001): Response of a Taipei Rapid Transit System (TRTS) tunnel to adjacent excavation. *Tunnunlling and Underground Space Technology*, vol. 16, no. 3, pp. 151-158.

Dassault Systèmes Simulia Corp. (2010): ABAQUS, user's manual. Providence, RI, USA.

Doležalová, M. (2001): Tunnel complex unloaded by a deep excavation. *Computers and Geotechnics*, no. 28, pp. 469-493.

Dunnicliff, J. (1993): *Geotechnical Instrumentation for Monitoring Field Performance.* New York: John Wiley & Sons Inc.

Glisic, B.; Inaudi, D. (2007): *Fibre Optic Methods for Structural Health Monitoring.* New York: John Wiley & Sons, Ltd.

Hefny, A.M.; Chua, H.C. (2006): An investigation into the behaviour of jointed tunnel lining. *Tunnunlling and Underground Space Technology*, vol. 21, no. 3-4, pp. 428-433.

Huang, H.W.; Xu, L.; Yan, J.L.; Yu, Z.K. (2006): Study on transverse effective rigidity ratio of shield tunnels. *Chinese Journal of Geotechnical Engineering*, vol. 28, no. 1, pp. 11-18. (in Chinese)

Huang, X.; Huang, H.W.; Zhang, D.M. (2012): Centrifuge modelling of deep excavation over existing tunnels. *Proceedings of the Institution of Civil Engineers: Geotechnical Engineering*, DOI: 10.1680/geng.11.00045.

Lee, K.M.; Ge, X.W. (2001): The equivalence of a jointed shield-driven tunnel lining to a continuous ring structure. *Journal of Canadian Geotechnical Engineering*, no. 38, pp. 461-483.

Lekhnitskii, S.G. (1981): *Theory of Elasticity of an Anisotropic Body.* Moscow: MIR Publishers.

Li, H.N.; Li, D.S.; Song, G.B. (2004): Recent applications of fiber optic sensors to health monitoring in civil engineering. *Engineering Structures*, vol. 26, no. 11, pp. 1647-1657.

Liu, H. L., Li, P., Liu, J. Y. (2011): Numerical investigation of underlying tunnel heave during a new tunnel construction. *Tunnelling and Underground Space Technology*, vol. 26, pp. 276-283.

Liao, S.M.; Peng, F.L.; Shen, S.L. (2008): Analysis of shearing effect on tunnel induced by load transfer along longitudinal direction. *Tunnelling and Underground*

Space Technology, vol. 23, pp. 421-430.

Metje, N.; Chapman, D.N.; Rogers, C.D.F.; Henderson, P.; Beth, M. (2008): An Optical Fiber Sensor System for Remote Displacement Monitoring of Structures– prototype Tests in the Laboratory. *Structural Health Monitoring*, vol. 7, no. 1, pp. 51-63.

Othonos, A.; Kalli, K. (1999): *Fiber Bragg Gratings: Fundamentals and Applications in Telecommunications and Sensing.* London: Artech House.

Peck, R.B. (1969): Deep excavations and tunneling in soft ground. *Proceedings of the 7th International Conference on Soil Mechanics and Foundation Engineering*, Mexico, State of the Art Volume, pp. 225-290.

Pellet, F. (2009): Contact between a tunnel lining and a damage-susceptible viscoplastic medium. *Computer Modeling in Engineering & Sciences (CMES)*, vol. 52, no. 3, pp. 279-295.

Samanta, A.K.; Ghosh, S. (2009): Bond-Slip Effects on the Behaviour of RC Beam under Monotonic Loading - An Integrated 3D Computational Model using EAS approach. *Computers, Materials & Continua*, vol. 12, no. 1, pp. 1-37.

Sharma, J.S.; Hefny, A.M.; Zhao, J.; Chan, C.W. (2001): Effect of large excavation on deformation of adjacent MRT tunnels. *Tunnunlling and Underground Space Technology*, vol. 16, pp. 93-98.

Shiba, Y.; Kawashima, K.; Obinata, N.; Kano, T. (1988): Evaluation of lining stiffness of shield tunnel in longitudinal direction in seismic analysis. *Proceedings of Japanese Civil Engineering Society*, pp. 319-327. (in Japanese)

Shivakumar, K.; Bhargava, A. (2004): Stress Concentrations Caused by Embedded Optical Fiber Sensors in Composite Laminates. *Computers, Materials & Continua*, vol. 1, no. 2, pp. 173-190.

Ullah, S.; Pichler, B.; Scheiner, S.; Hellmich, C. (2010): Shell-specific interpolation of measured 3D displacements, for micromechanics-based rapid safety assessment of shotcrete tunnels. *Computer Modeling in Engineering & Sciences (CMES)*, vol. 57, no. 3, pp. 279-316.

Yin, J.H.; Zhu, H.H.; Fung, K.W. (2008): Innovative Optical Fiber Sensors for Monitoring Displacement of Geotechnical Structures. *Proceedings of the HKIE Geotechnical Division Annual Seminar 2008*, Hong Kong, China, pp. 287-294.

Yin, J.H.; Zhu, H.H.; Pei, H.F.; Hong, C.Y. (2010): Fiber optic based monitoring and warning of safety operation of super-long tunnel. *8th Cross-strait Seminar on Bridge and Tunnel Engineering,* Fu Zhou, China, pp. 140-147. (in Chinese)

Zhang, D.M.; Huang, H.W. (2009): Monitoring and modelling of riverside large deep excavation-induced ground movements in clays. *Geotechnical Aspects of Un-*

derground Construction in Soft Ground, Taylor and Francis Group, London, pp. 215-221.

Zhang, D.M.; Ma, L.X.; Huang, H.W.; Zhang, J. (2012): Predicting leakage-induced settlement of shield tunnels in saturated clay. *Computer Modeling in Engineering & Sciences (CMES)*, vol. 89, no. 3, pp. 163-188.

Zhou, B.; Xie, X.Y.; Yang, Y.B.; Jiang, J.C. (2012): A novel vibration-based structure health monitoring approach for the shallow buried tunnel. *Computer Modeling in Engineering & Sciences (CMES)*, vol. 86, no. 4, pp. 321-348.

Zhu, H.H.; Ho, A.N.L.; Yin, J.H.; Sun, H.W.; Pei, H.F.; Hong, C.Y. (2012): An optical fiber monitoring system for evaluating the performance of a soil nailed slope. *Smart Structures and Systems*, vol. 9, no. 5, pp. 393-410.